Multiple Structural Coloring of Silk-Fibroin Photonic Crystals and Humidity-Responsive Color Sensing

Ying Ying Diao, Xiang Yang Liu, Guoyang William Toh, Lei Shi, and Jian Zi*

In the biological world, numerous creatures such as butterflies, insects, and birds have exploited photonic structures to produce bicolor reflections with important biofunctions in addition to unique brilliant structural coloration. Although the mimicking of bistructural color reflection is possible, the fabrication involves a process of combined layer deposition techniques, which is complicated and less flexible. Here, a bistructural color mimicking, based on silk fibroin, is reported using a simple and inexpensive self-assembly method. Silk-fibroin inverse opals with different spectral positions of bistructural color reflection (i.e., ultraviolet and visible peaks, ultraviolet and near infrared peaks, and visible and near infrared peaks) are obtained by simply controlling their lattice constants. Furthermore, the inline and continuous tuning of the peak positions of bistructural color reflection can be achieved by the humidity-induced cyclic contraction of silk fibroin. The potential applications of silk-fibroin photonic structures in eco-dying and multifunctional silk fabrics are also demonstrated.

1. Introduction

Structural coloration caused by the interaction of light with nanoscale periodic structures, so-called photonic crystals, has attracted considerable attention in a variety of research areas recently.[1] Besides the relevancy to the display and sensing technologies,[2,3] the implement of structural colors to fabrics will bring revolutionary changes to the textile industry. Structural color has many characteristics that differ from those of pigments or dyes. The unique colors originating from the physical structures are usually iridescent or metallic and cannot be obtained by chemical dyes or pigments. Moreover, structural color is brighter, more deeply saturated, free from photobleaching, and longer lasting, unlike traditional pigments or dyes.[4] Incorporating structural color in fabrics may revolutionize the eco-dying technologies in textile industries and, therefore, research in this area has attracted enormous attentions.[5–7]

In the biological world, the colorful feathers of many birds (i.e., peacocks), the wings of various butterflies,and the elytra of many beetles are good examples of structural coloration.[4,8–11] Apart from the aforementioned properties, natural structural colors produced by these animals also give rise to additional optical properties. For instance, the brown barbules of peacock feathers adopt mixed structural coloration;[11] the green wing scales of *Papilio Blumei* produce polarization effect and bistructural colors.[6,12] In particular, bistructural colors are responsible for crucial functions in the animal kingdom. The widespread evidence indicates that animal photoreceptors can distinguish different parts of the spectrum, even also sensitive to UV light.[13] It follows that the bistructural colors of certain butterflies cover both the visible and UV ranges, which may serve as communication and mating signals.[14,15] Evidently, the construction of an effective and simple way to produce multiple structural colors simultaneously covering the UV, visible, and infrared (IR) ranges may point to a new direction in multifunctional photonic materials engineering. Note that although there have been numerous attempts to mimic natural structural colors,[16–25] not much attention has been focused on the bistructural colors.

Bistructural colors can be created by different manners in the biological world.[12,26,27] **Figure 1**a depicts the bistructural colors created by the blue wing scales of the butterfly *Papilio Ullysess* (*P. Ullysess*). Under UV-visible light, the blue wing scales display two distinct reflection peaks. Specifically, the concavities of a multilayer structure and the ridges of a 2D photonic-crystal structure occurring at the wing scales produce green and UV reflections, respectively.[27] On the other hand, the green wing scales of the butterfly *Papilio Blumei* (*P. Blumei*) produce the reflections of two different visible colors. As shown in Figure 1b, the yellow and blue reflections created by the flat bottoms and inclined sides of the concavities, respectively, give rise to a color mixing, leading to a green color that is perceived by human eyes. The aforementioned bistructural colors produced by the two *Papilio* butterflies are of different structural origins: in *P. Ullysess* it is produced by two different types of ordered structures of the wing scales, while

Prof. X. Y. Liu
Research Institute for Biomimetics and Soft Matter
College of Materials
Xiamen University
422 Si Ming Nan Road, Xiamen 361005, PR China
Dr. Y. Y. Diao, Prof. X. Y. Liu, G. W. Toh
Department of Physics and the Department of Chemistry
National University of Singapore
2 Science Drive 3, Singapore 117542
E-mail: liuxy@xmu.edu.sg
Dr. L. Shi, Prof. J. Zi
Department of Material Science
Fudan University
220 Handan Road, Shanghai, China 200433

DOI: 10.1002/adfm.201203672

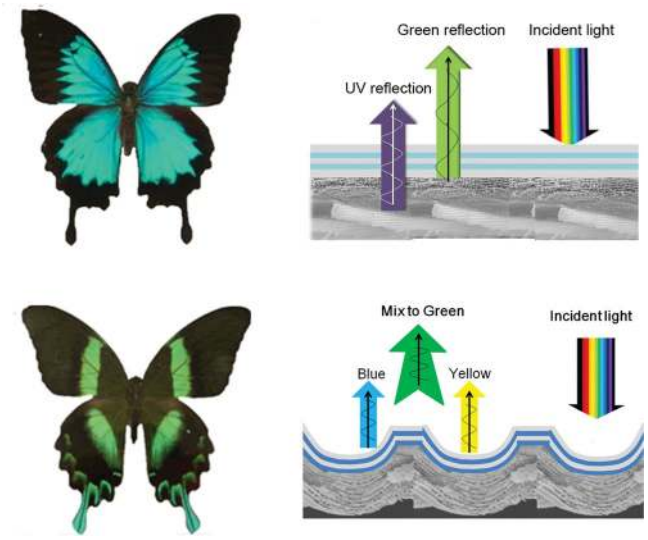

Figure 1. Bistructural colors produced by two species of *Papilio* butterflies. a) *P. Ullysess.* The blue scales (i) give rise to two reflection peaks; one is located in the UV range and is produced by the ridges and the other (green reflection) is located in the visible range and is produced by the concavities (ii). b) *P. Blumei.* The green scales (i) generate a bistructural colors with the flat parts of the concavities reflecting yellow light and the inclined sides of the concavities reflecting blue light (ii).

in *P. Blumei* it is produced by the different illumination angles from different parts of the wing scales, which share the same ordered nanostructure.

Although it is possible to mimic the sophisticated nanostructures of *P. Blumei* in a well-controlled manner to obtain the bireflection structural colors by a combined layer deposition technology,[16] a cost-effective manufacturing scheme to generate bistructural colors over a large area is hard to achieve because of the complicity of fabrication and precision of control. Here, we present a new approach to design and construct biomaterials of bistructural colors in a single inverse opal photonic structure by taking advantage of the particular photonic band structure of this type. This overcomes the limitations of previous approaches and makes it possible to tune the wavelengths of bistructural colors peaks easily. The material to be adopted in this work is silk fibroin, which has recently emerged as a highly promising biomaterial in the applications of biomedicine, biophotonics/electronics, etc., owing to its excellent mechanical and optical properties, biocompatibility, biodegradability, and implant ability.[28–32] In this regard, the rapid production of silk fibroin inverse opals with bistructural colors in both UV and visible (UV/visible), visible and IR (visible/IR), and UV and IR (UV/IR) ranges is demonstrated. We implement the control of the wavelengths of bistructural color reflection peaks i) by adjusting the structural parameters of silk inverse opals and ii) via the special property of silk fibroin: humidity induced cyclic contraction.[33] The latter is considered to mimic the structural color changes found in longhorn beetles.[34] Due to the multistructural reflection nature, this can give rise to the humidity response in multiple wavelengths.

2. Results and Discussion

In analogy to electron waves in a solid crystal, light propagation in photonic crystals is characterized by photonic band structure.[35] If refractive-index modulations in photonic crystals are sufficient, a photonic bandgap can open up. For frequencies within this photonic bandgap, light propagation is not allowed. To show that a silk fibroin inverse opal can produce bistructural colors, its photonic band structure is calculated by a plane-wave expansion method,[36,37] as shown in **Figure 2**a. In the calculations, the silk fibroin inverse opal is assumed to consist of air spheres arranged in a face-centered cubic (FCC) lattice with silk fibroin filled in the remaining regions. The refractive index, n, of silk fibroin is 1.54.[38] Obviously, there is no complete (for all directions) photonic bandgap due to the fact that the refractive-index contrast between silk fibroin and air is not big enough. However, along the Γ-L direction in the first Brillouin zone of the FCC lattice, there exist two partial photonic bandgaps at different frequencies. For light incident along the Γ-L direction strong reflections are expected for frequency within the two partial photonic bandgaps, leading to bistructural colors

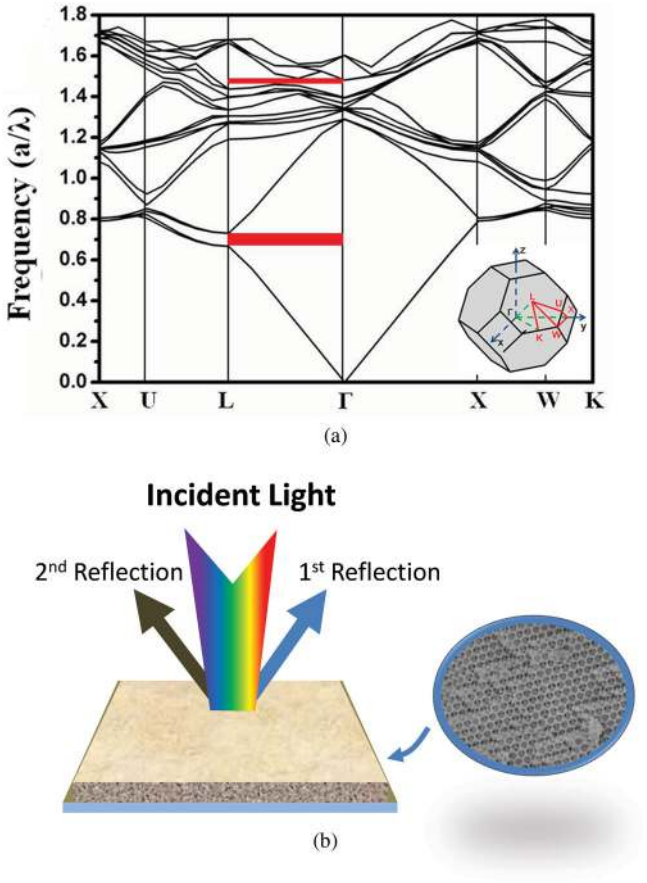

Figure 2. a) Calculated photonic band structure of a silk fibroin inverse opal along the high-symmetrical directions in the first *Brillouin* zone. Frequency is in units of a/λ, where a is the lattice constant of the inverse opal and λ is the wavelength in vacuum. Two partial photonic band gaps (red regions) exist along the Γ-L direction. The inset is the first *Brillouin* zone of the FCC lattice. b) Schematic of bistructural colors from a silk-fibroin inverse opal.

at two different frequency or wavelength ranges. Note that the midgap frequencies of both partial photonic band gaps increase along the direction from *L* to *U*, suggesting that the resulting bistructural colors are iridescent; in other words, the two reflection peaks will undergo a blue shift in wavelength for light incidence varying away from the *Γ*-*L* direction.

Evidentally, we can implement the following approach to adjust the bistructural colors offered by inverse opals. i) For an inverse opal, the positions of the two peaks (λ_1 and λ_2) and their separation between them ($\Delta\lambda$) can be adjusted by changing the lattice constant *a* since the midgap frequencies are inversely proportional to *a*. ii) Once the lattice constant *a* is given, λ_1, λ_2 and $\Delta\lambda$ can be adjusted by changing the refractive indices of the constituent materials. iii) If *a* and constituent materials are given, λ_1, λ_2 and $\Delta\lambda$ can be changed by varying the illumination angle, similar to the case indicated for *P. Blumei*.

For a silk fibroin inverse opal, the midgap wavelength of the first partial photonic bandgap is at $\lambda_1 = 1.429a$, that of the second partial photonic bandgap occurs at $\lambda_2 = 0.685a$, and their separation is $\Delta\lambda = 0.744a$ (for more details see Experimental Section). Therefore, to obtain a silk fibroin inverse opal with visible/IR reflection peaks, the first peak ($\lambda_1 = 1.429a$) should be located within the IR region (>700 nm) and the second ($\lambda_2 = 0.685a$) should fall into the visible region (400–700 nm) (Figure 2b). In this case, a suitable lattice constant (584 nm < *a* < 1022 nm) should be adopted. Similarly, we can obtain silk-fibroin inverse opals with UV/IR or UV/visible reflection peaks by adopting corresponding lattice constants.

The procedure for fabricating silk-fibroin inverse opals is illustrated in **Figure 3**a. First, a regenerated silk fibroin solution (1–4% w/v) is prepared by raw silk fibers[39] (see Experimental Section for more details). Second, colloidal crystals with the FCC structure are grown from monodispersed polystyrene colloidal spheres with a proper size, in order to create templates for producing silk-fibroin inverse opals.[40] The growth of colloidal crystals on a given substrate is one of the rate determining steps to acquire silk-fibroin inverse opal films, which is achieved through an evaporation-induced self-assembly process.[41,42] Third, the regenerated silk-fibroin solution is cast and penetrated into the voids of the colloidal crystals. Finally, the templates are removed by chemical etching to obtain the silk fibroin inverse opal films (refer to Experimental Section).

Figure 3b shows the scanning electron microscopy (SEM) images of a colloidal crystal template and a resulting silk-fibroin inverse opal fabricated using 700 nm colloidal spheres. The sharp peaks in the FFT pattern (the inset of Figure 3b(i)) indicate that the quality of the FCC colloidal crystal is high. The SEM images of the silk-fibroin inverse opal at low and high magnifications are displayed in Figure 3b(ii,iii), respectively, which show the highly ordered hexagonal structure. The sharp FFT pattern (the inset of Figure 3b(ii)) also verifies the high quality of the inverse opal. The inset of Figure 3b(iii) displays the details of one cavity in the inverse opal structure, where the three channels connecting to the adjacent pores can be seen. This is the corresponding structure giving rise to the

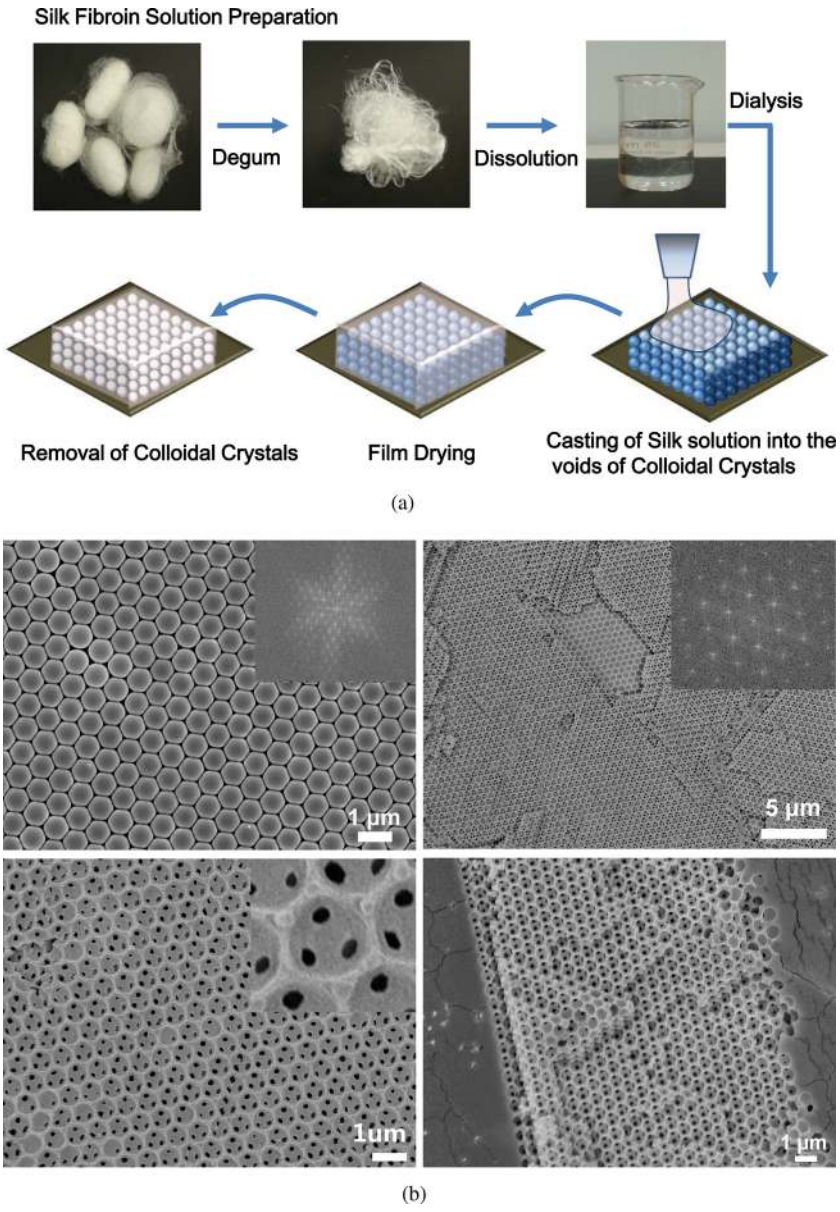

Figure 3. a) Procedure for fabricating silk-fibroin inverse opals. b) SEM images of colloidal crystal and silk-fibroin inverse opal fabricated by 700 nm colloidal spheres: i) SEM images of the colloidal crystal, the inset shows the fast Fourier transformation (FFT) pattern. ii,iii) Images of the silk-fibroin inverse opal with low and high magnifications. The inset in (ii) is the FFT pattern of the inverse opal structure. The inset in (iii) is the detailed structure of one cavity of the inverse opal structure. iv) Transverse cross section structure of the silk-fibroin inverse opal.

bistructural colors in the photonic crystals.[43,44] The transverse cross-section shown in Figure 3b(iv) indicates that the thickness of the obtained silk-fibroin inverse opal is about 20 layers of ordered hollow silk-fibroin spheres. Notice that while the cracking is a common issue in other inverse opals, silk-fibroin inverse opals display significantly improved perfection and the enhanced rupture/crack resistance due to the elastic nature of silk fibroin.[45]

In the following, we demonstrate that we can attain silk-fibroin inverse opals with bistructural colors located at UV/visible, UV/IR, and visible/IR. In this regard, polystyrene colloidal spheres with different diameters (350 nm, 450 nm, 500 nm, and 700 nm) are chosen. Fabricated silk-fibroin inverse opals are characterized both spectrally and optically (**Figure 4**). The first example is a silk-fibroin inverse opal fabricated with 350 nm colloidal spheres. As shown in Figure 4a, two reflection peaks exist with one at UV (≈285 nm) and the other at the visible (≈590 nm), showing an orange structural color to our perception. The separation between the two peaks is $D\lambda$ = 310 nm. The 450 nm silk fibroin inverse opal (Figure 4b) gives rise to one peak located in the UV range (≈380 nm) and the other in the near IR range (≈800 nm). Both are invisible to the human eye. The bistructural colors of the 500 nm silk fibroin inverse opal (Figure 4c) shows that one peak is located in the visible (≈430 nm) and the other in the near IR (≈870 nm). The visible reflection peak gives rise to a purple structural color. The 700 nm silk/fibroin inverse opal (Figure 4d) should display two reflection peaks with one peak (≈620 nm) in the visible, producing a red color and the other in IR, which is beyond the detection range of our spectrometer.

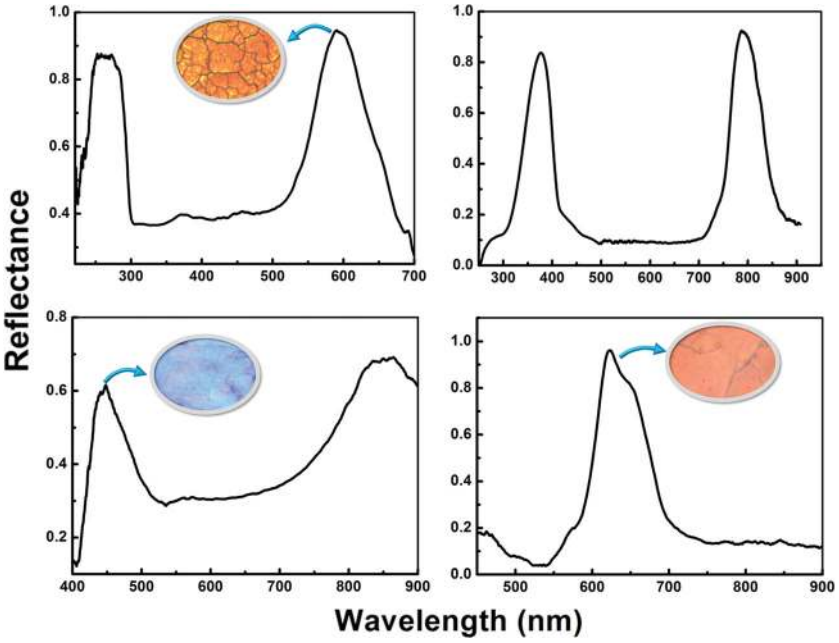

Figure 4. The measured bistructural color reflectance spectra. a–d) Reflectance spectra for silk-fibroin inverse opals fabricated by 350 nm, 450 nm, 500 nm, and 700 nm colloidal spheres, respectively. The insets of (a,c,d) are the orange, purple, and red colors observed under an optical microscope for 350 nm, 500 nm, and 700 nm silk-fibroin inverse opals, respectively.

As discussed before, the partial photonic bandgaps are direction dependent. The two peaks of the bistructural colors should undergo a blue shift in wavelength with the incident angle changing from normal to oblique. Our experimental results show that as the incident light angle increases, the double reflection peaks would undergo a blue-shift.[42] For the 700 nm silk-fibroin inverse opal, its angular reflection spectra are measured at different incident angles (0°–60°) with respect to the normal of the (111) plane (Figure S1, Supporting Information). The 620 nm peak under normal incidence disappears quickly as θ increases to 15°, where θ is the incident angle. With the further increment of incident angle, another peak appears once θ reaches 45°. Both peaks undergo a blue shift with the increment of incident angle. The blue shift of the reflection peaks can be understood by the fact that the two partial photonic bandgaps increase their midgap frequency along the *L*-*U* direction, implying that the resulting reflection peaks should shift to low wavelengths with the increment of incident angle.

Silk-fibroin inverse opals prepared by polystyrene colloidal spheres of different diameters have the same FCC structure, except the lattice constant. We notice that although the radius of the air spheres in a silk-fibroin inverse opal is determined to a large extent by the radius of colloidal spheres, the SEM images reveal that the actual size of air spheres shrinks about 10–20% compared with the size of colloidal spheres, which also occurs in the preparation of other porous materials.[46] One consequence is that we have to consider the shrink of the lattice constant in the design of a silk fibroin inverse opal. Moreover, when comparing the measured reflection peaks with the calculated midgap wavelengths of the partial photonic bandgaps along the *Γ*-*L* direction, we should take the measured lattice constant. **Table 1** gives the measured lattice constant of

Table 1. Measured lattice constant and comparison of the measured and calculated reflection peaks.

Samples	Measured lattice constant	Calculated midgap wavelength		Measured reflection peaks
		λ_1 (1.429*a*)	λ_2 (0.685*a*)	
350 nm inverse opal	415 nm	592 nm	284 nm	285 nm and 590 nm
450 nm inverse opal	560 nm	810 nm	383 nm	380 nm and 800 nm
500 nm inverse opal	620 nm	885 nm	424 nm	430 nm and 870 nm
700 nm inverse opal	900 nm	1285 nm	616 nm	620 nm

fabricated silk-fibroin inverse opals and corresponding predicted and measured reflection peaks. It is obvious that the predicted reflection peaks agree well with the measured ones. This indicates ambiguously that the bistructural color reflection in silk-fibroin inverse opals stems indeed from the two partial photonic bandgaps along the *Γ-L* direction.

As discussed, the two reflection peaks of a silk-fibroin inverse opal can be altered by changing its lattice constant, namely the size of colloidal spheres. Nevertheless, for a ready-made silk-fibroin inverse opal, tuning the reflection peaks is an important issue. In the following, we will present a simple and effective approach to tune the reflection peaks by external stimuli.[44] In this regard, we will take the advantages of silk fibroin to achieve responsive silk-fibroin inverse opals.

It was reported that both spider silk and silkworm silk show a so-called humidity-induced cyclic contraction property.[33] This results in the expanding and contraction of silks at different humidity levels. A high humidity gives rise to the infiltration of water molecules into the silk fibers. Water molecules first bind themselves to the random coils within the amorphous region of silk disrupting the relatively weak hydrogen bonding. This relaxes the silk and gives rise to the dip in the stress–strain curve. Upon drying, water molecules are lost only from the random coil region, rebuilding hydrogen bonds in the process that immobilize the silk molecules, contracting the fibers.

Regenerated silk films preserve most if not all the compositions of silkworm silk. Thus cyclic contraction should be also observed in a regenerated silk-fibroin film. To control humidity, samples are put into a humidity chamber. The tensile stress, reflection spectra, and optical microscope images are directly obtained by a micromechanical tester and an optical microscope, which is connected to a spectrometer (**Figure 5**a). Using the setup illustrated in Figure 5a(i), the mechanical response, tensile stress of a silk fibroin film at low (30% RH) and high (80% RH) humidity levels is measured (Figure 5b, blue curve). The test begins at a lower humidity level, initial drying induces a stress (contraction) of ≈5 MPa. The film then relaxes back to its original tension as humidity is subsequently increased and the cycle repeats itself. It follows that the silk-fibroin film does not show obvious fatigue even after approximate 6500 s (three repetitions) under tension.

The reflection spectra and optical microscope images of a 350 nm silk-fibroin inverse opal are obtained using the setup illustrated in Figure 5a(ii). Our results indicate that the humidity induced cyclic contraction of silk-fibroin films can be utilized to precisely control the optical property of silk-fibroin inverse opals. As shown in Figure 5b (red curve), the visible reflection peak of the 350 nm silk-fibroin inverse opal exhibits a red shift with increasing humidity level. At a high humidity level, the decrease of the tensile stress would induce the swelling of silk fibroin, leading to the expansion of the silk-fibroin shells in the inverse opal (as illustrated in the inset of Figure 5d). Besides, the water infiltration would change the refractive indices of the silk-fibroin shells and air spheres.[45] Therefore, the red-shift of the visible reflection peak of the 350 nm silk-fibroin inverse opal results from the water infiltration induced the swelling of silk-fibroin shells and the changes of refractive indices. On contrary, the reflection peak of the silk-fibroin inverse opal exhibits a blue shift with lowering of the humidity level, allowing for precise tuning of the reflection peak of a silk-fibroin inverse opal within a certain range. During the cyclic process, the shift of the reflection peak is also reversible.

The reflection spectrum of the sample under different humidity levels (from 30% to 80% with step increment of 10%; Figure S2, Supporting Information) is recorded. Figure 5c shows that the optical microscopy images of 350 nm silk-fibroin inverse opal under 80% and 30% humidity levels. The blue-shift is further proven by the structural color change from orange to yellow color. The structural color change in silk-fibroin inverse opals at different humidity levels is quite similar to that of longhorn beetles *Tmesisternus isabellae*.[34] The reflectance spectrum for the UV peak of 350 nm silk-fibroin inverse opal under different humidity levels is also measured. As shown in Figure 5d, the reflection peaks of the silk-fibroin inverse opal decrease almost linearly with lowering humidity level. The visible reflection peak of 350 nm silk-fibroin inverse opal shifts from 603 nm to 587 nm, and the UV peak shifts from 291 nm to 285 nm with lowering the humidity level from 80% to 30%. Due to its biocompatibility and degradability, silk fibroin has been widely applied in the biomedical area, i.e., artificial skin, scaffolds for tissue engineering, biocoatings, etc., and the creation of the inverse opal structure of the materials may add biosensors in vivo. In addition, the tuning of the reflection peaks of silk-fibroin inverse opal may be used as compatibility optical switches, active video displays, and rewritable paper in the future.

Silkworm silk has been adopted as textile materials for more than 7000 years. To fabricate the opal and inverse opal structures onto silk fabrics to produce vivid structural colors will revolutionize the eco-dying industry. By coating the silk photonic crystals onto the surface of fabrics, we can produce multifunctional fabrics in addition to the vivid structural colors.[5] For instance, we can acquire the UV protective textiles by adjusting one of the reflection peaks into the UV range. Similarly, the thermal insulating performance can be achieved by locating one of the reflection peaks into the IR range, which will create auto-cooling textiles in a hot summer if the structure is generated in the outer layer of textiles. On the other hand, it will preserve body heat in a cold winter if the IR reflecting structure is generated in the inner layer of textiles.

The UV, visible, and near-IR reflection peaks indicate the potential applications of structural colors in eco-dying engineering, UV protection, and IR radiation shielding. Photonic crystals consisting of polystyrene spheres arranged in an ordered FCC structure can be fabricated on the surface of silk fabrics (**Figure 6**, see Experimental Section). As mentioned, different reflection peaks (UV, visible, and IR) produced by the photonic crystals can be achieved through changing the size of colloidal spheres (Figure S3, Supporting Information). As two examples, the red and golden colored silk fabrics in Figure 6 are fabricated using 270 nm and 240 nm self-assembled colloidal crystals, respectively.

3. Conclusions

In summary, a simple and highly effective scheme based on silk-fibroin photonic crystals with the inverse opal structure is

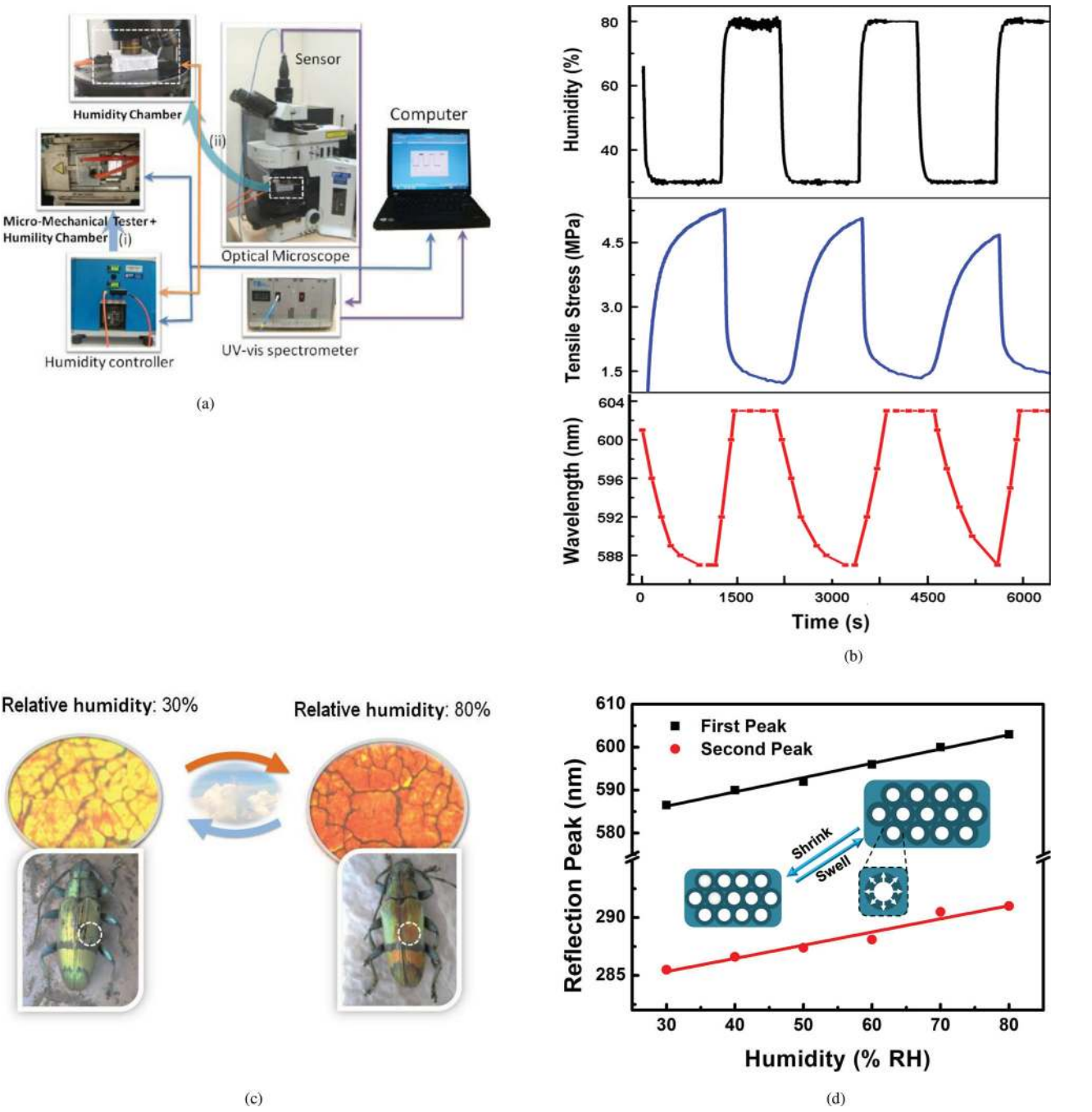

Figure 5. Control and tune of the reflection peaks of silk fibroin inverse opals by humidity. a) Experiment setup for the measurements of the cyclic contraction of silk-fibroin film (i) and the corresponding optical properties of silk fibroin inverse opal (ii). b) The cyclic tensile stress of the silk-fibroin film in response to the humidity change (blue curve); the measured reflection peaks for 350 nm silk-fibroin inverse opal with changes of humidity levels (red curve). c) The color of silk-fibroin inverse opals under optical microscopy changes from orange at 80% humidity level to yellow at 30% humidity level, illustrating the biomimetic of the humidity responsive structural color of beetle. d) Linear relationship between the reflection peaks and humidity levels.

proposed to produce bistructural colors. Such a scheme takes advantage of two partial photonic bandgaps of inverse opals. The positions of the two reflection peaks, as well as their separation can be simply adjusted by changing the lattice constant of the inverse opal structure. The silk-fibroin inverse opal films with the bistructural colors covering UV/visible, UV/IR, and visible/IR regions are fabricated. Moreover, the reflection peaks of a ready-made silk-fibroin inverse opal can be tuned through the change in the humidity level based on the cyclic contraction of silk fibroin. The strategies of fabricating silk-based photonic crystals in eco-dying and multifunctionalizing silk fabrics are discussed.

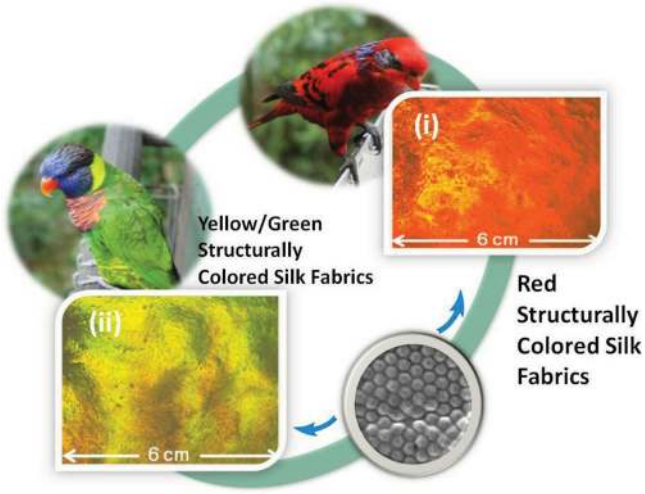

Figure 6. Creation of structural color to silk fabrics. Silk fabrics with structural color, wherein the colloidal crystals were fixed on the surface of silk fabrics by silk-fibroin solution, were created. The two examples of silk fabrics with structural red (i) and golden (ii) colors were fabricated using 240 nm and 270 nm self-assembled colloidal crystals, respectively.

4. Experimental Section

Materials: *P. Ullysess* and *P. Blumei* were acquired from the Insets and Butterfly Kingdom of Singapore. Silkworm cocoons were harvested from laboratory-fed silkworm *Bombyx mori*.

Silk Fibroin Solution Preparation: The production of silk fibroin solution has been previously documented.[39] In general, it began with the purification of harvested cocoons. Sericin was removed from the fibroin strands by boiling the cocoons in a 0.5 wt% aqueous solution of sodium biocarbonate for 45 min. Then, the fibroin bundle was rinsed thoroughly in deionized (DI) water several times and allowed to dry overnight. The dried silk fibroin was dissolved in a saturated solution of lithium bromide (9.3 M) at 40 °C for 1 h. The lithium bromide salt was then extracted from the solution through a water-based dialysis cassette for 3 days. Remaining particulates were removed through centrifugation (10 000 rpm, 15 min). The whole process produced 4% w/v silk-fibroin solution with excellent quality and stability. The required 2% w/v solution was obtained by diluting the original one.

Calculation of the Band Structure of Silk-Fibroin Inverse Opals: The numerical simulations were carried out using commercial software (RSoft Design). The first 20 bands were calculated for the first Brillouin zone of the FCC lattice. As a silk fibroin inverse opal consists of hollow silk fibroin spheres, the thickness of silk fibroin shells (d_1) was assumed to be 10% with respect to that of air spheres (d_2). The refractive index of silk fibroin was taken as 1.54.[38] There are two partial PBGs in the calculated band structure of silk fibroin inverse opal, the midgap frequency of the 1st stop gap is at $a/\lambda = 0.7$, and that of the 2nd stop gap occurs at $a/\lambda = 1.46$.

Fabrication of Silk Fibroin Inverse Opals: The templates used were 3D colloidal crystals. Monodispersed polystyrene (PS) latex spheres with different diameters (350 nm, 450 nm, 500 nm, and 700 nm) were used as received from the supplier (Duke Scientific). The colloidal suspensions were loaded on silica substrates, and dense colloidal crystals were grown by sedimentation of the spheres. The samples were dried at 40 °C for 2–4 h. Colloidal crystals formed with the evaporation of the suspensions.[41,42] In the next step, the voids in the colloidal crystals were filled with silk fibroin. The diluted (1–4% w/v) silk-fibroin solution was casted and penetrated into voids of the colloidal crystals by capillary force. The samples were then incubated (25 °C, 30% relative humidity) for 5 h, ensuring the voids in the colloidal crystal were sufficiently filled and allowing the silk fibroin solution to dry slowly. In the third step of the process, PS spheres were removed by immerse the samples into tetrahydrofuran (THF; Fluke) for 4–5 h. And then the samples were taken out to evaporate the THF.

Fabrication of Silk Photonic Crystals on the Surface of Silk Fabrics: A PS colloidal suspension was loaded onto the surface silk fabric. The colloidal crystal was then self-assembled on the silk fabric surface. Afterwards, silk-fibroin solution was loaded to fix the colloidal crystals to the surface of silk fabric.

Characterization of the Synthesized Colloidal Crystals and Silk-Fibroin Inverse Opals: A field-emission scanning electron microscope (SEM-JEOL 6700F) was used to characterize the microstructures of the samples. The silk-fibroin inverse opals were putting into liquid nitrogen and then cut into pieces, the transverse cross-section images were then characterized by SEM. Optical images were taken using an Olympus (BX 61), reflectance measurements were carried out by UV-Vis spectrometer (Ocean Optics 2000) and a homemade angle-resolved reflectance spectrometer.

Cyclic Contraction Measurement of Silk Fibroin Film: To measure the stress generated by the silk-fibroin film under changing humidity levels, a silk-fibroin film (thickness: 0.1 mm, width: 1.5 mm) fabricated by drying regenerated silk fibroin solution was adhered to cardboard mounts across 20 mm gaps. Measurements of stress were performed using Instron S5762A (Model 5525X Mini Horizontal Test System) with a 0.5 N load cell. The Instron was custom fit with a home-built chamber that controlled humidity with a range of ≈30–80% RH. Humidity in the environmental chamber was regulated by the triton technology humidity generator and controller. The reflectance spectra of 350 nm silk-fibroin inverse opal were measured by placing the sample in the custom humidity-controlled chamber and subsequently recorded the spectra.

Supporting Information

Supporting Information is available from Wiley Online Library or from the author.

Received: December 12, 2012
Published online: May 27, 2013

[1] S. Berthier, *Iridescences: The Physical Colours of Insects*, Springer, New York **2007**.
[2] A. C. Arsenault, H. Miguez, V. Kitaev, G. A. Ozin, I. Manners, *Adv. Mater.* **2003**, *15*, 503.
[3] A. C. Arsenault, D. P. Puzzo, I. Manners, G. A. Ozin, *Nat. Photonics* **2007**, *1*, 468.
[4] S. Kinoshita, S. Yoshioka, *ChemPhysChem* **2005**, *6*, 1442.
[5] X. Y. Liu, Y. Y. Diao, US patent, *SG-810110-01-SG-PCT* **2011**.
[6] Y. Y. Diao, X. Y. Liu, *Adv. Funct. Mater.* **2012,** *22*, 1354.
[7] X. Y. Liu, Y. Y. Diao, US patent, *SG-821277-01-US-REG*, **2012**.
[8] S. Banerjee, Z. Dong, *Opt. Rev.* **2007**, *14*, 359.
[9] J. Zi, X. Yu, Y. Li, C. Hu, C. Xu, X. Wang, X. Liu, R. Fu, *Proc. Natl. Acad. Sci. USA* **2003**, *100*, 12576.
[10] S. Kinoshita, *Structural Colours in the Realm of Nature*, World Scientific Publishing, Singapore **2008**.
[11] Y. Z. Li, Z. Lu, H. Yin, X. Yu, X. Liu, J. Zi, *Phys. Rev. E* **2005**, *72*, 010902.
[12] P. Vukusic, J. R. Sambles, C. R. Lawrence, *Nature* **2000**, *404*, 457.
[13] A. D. Briscoe, S. M. Bybee, G. D. Bernard, F. Yuan, M. P. Mangus, R. D. Reed, A. D. Warren, J. L. Bousquets, C. C. Chiao, *Proc. Natl. Acad. Sci. USA* **2010**, *107*, 3628.
[14] M. L. M. Lim, M. F. Land, D. Q. Li, *Science* **2007**, *315*, 481.
[15] Y. Takeuchi, K. Arikawa, M. Kinoshita, *J. Exp. Biol.* **2006**, *209*, 2873.

[16] M. Kolle, P. M. Salgard-Cunha, M. R. J. Scherer, F. Huang, P. Vukusic, S. Mahajan, J. J. Baumberg, U. Steiner, *Nat. Nanotechnol.* **2010**, *5*, 511.
[17] J. Y. Huang, X. D. Wang, Z. L. Wang, *Nano. Lett.* **2006**, *6*, 2325.
[18] Y. Chen, J. Gu, S. Zhu, T. Fan, D. Zhang, Q. Guo, *Appl. Phys. Lett.* **2009**, *94*, 053901.
[19] H. L. Ge, Y. L. Song, L. Jiang, D. B. Zhu, *Thin Solid Films* **2006**, *515*, 1539.
[20] R. G. Xie, X. Y. Liu, *J. Am. Chem. Soc.* **2009**, *131*, 4976.
[21] J. E. G. J. Wijnhoven, W. L. Vos, *Science* **1998**, *281*, 802.
[22] H. Kim, J. Ge, J. Kim, S. Choi, H. Lee, H. Lee, W. Park, Y. Yin, S. Kwon, *Nat Photonics* **2009**, *3*, 534.
[23] O. D. Velev, E. W. Kaler, *Adv. Mater.* **2000**, *12*, 531.
[24] L. Cao, P. Fan, E. S. Barnard, A. M. Brown, M. L. Brongersma, *Nano Lett.* **2010**, *10*, 2649.
[25] T. Khudiyev, E. Ozgur, M. Yaman, M. Bayindir, *Nano Lett.* **2011**, *11*, 4661.
[26] P. Vukusic, R. Sambles, C. Lawrence, G. Wakely, *Appl. Opt.* **2001**, *40*, 1116.
[27] Y. Y. Diao, X. Y. Liu, *Opt. Express* **2011**, *19*, 9232.
[28] N. Du, X. Y. Liu, J. Narayanan, L. Li, M. L. M. Lim, D. Li, *Biophys. J.* **2006**, *91*, 4528.
[29] C. Jiang, X. Wang, R. Gunawidjaja, Y. H. Lin, M. K. Gupta, D. L. Kaplan, R. R. Naik, V. V. Tsukruk, *Adv. Funct. Mater.* **2007**, *17*, 2229.
[30] M. K. Gupta, S. Singamaneni, M. Mcconney, L. F. Drummy, R. R. Naik, V. V. Tsukruk, *Adv Mater.* **2010**, *22*, 115.
[31] F. Vollrath, D. P. Knight, *Nature* **2001**, *410*, 541.
[32] G. H. Altman, C. Jakuba, T. Calalro, R. L. Horan, J. Chen, H. Lu, J. Richmond, D. L. Kaplan, *Biomaterials* **2003**, *24*, 401.
[33] I. Agnarsson, A. Dhinojwala, V. Sahni, T. A. Blackledge, *J. Exp. Biol.* **2009**, *212*, 1990.
[34] F. Liu, B. Q. Dong, X. H. Liu, Y. M. Zheng, J. Zi, *Opt. Express* **2009**, *17*, 16183.
[35] E. N. Economou, M. M. Sigalas, *Phys. Rev. B* **1993**, *48*, 13434.
[36] J. D. Joannoupoulos, R. D. Meade, J. N. Winn, *Photonic Crystals: Molding the flow of light*, Princeton University Press, Princeton **2008**.
[37] N. W. Ashcroft, N. D. Mermin, *Solid State Physics*, Holt, Rinehart and Winston, New York **1976**.
[38] B. D. Lawrence, M. Cronin-Golomb, I. Georgakoudi, D. L. Kaplan, F. G. Omenetto, *Biomacromolecules* **2008**, *9*, 1214.
[39] M. K. Sah, K. Pramanik, *Int. J. Environ. Sci. Dev.* **2010**, *1*, 404.
[40] V. M. Swinerd, A. M. Collins, N. J. V. Skaer, T. Gheysens, S. Mann, *Soft Matter* **2007**, *3*, 1377.
[41] V. N. Bogomolov, S. V. Gaponenko, I. N. Germanenko, A. M. Kapitonov, E. P. Petrov, N. V. Gaponenko, A. V. Prokofiev, A. N. Ponyavina, N. I. Silvanovich, S. M. Samoilovich, *Phys. Rev. E* **1997**, *55*, 7619.
[42] W. L. Vos, R. Sprik, A. V. Blaaderen, A. Imhof, A. Lagendijk, G. H. Wegdam, *Phys. Rev. B* **1996**, *53*, 16231.
[43] W. L. Vos, H. M. van Driel, *Phys. Lett. A* **2000**, *272*, 101.
[44] N. P. Johnson, D. W. McComb, A. Richel, B. M. Treble, R. M. De la Rue, *Synth. Met.* **2001**, *116*, 469.
[45] K. Nakamae, T. Nishino, H. Ohkubo, *Polymer* **1989**, *30*, 1243.
[46] D. Y. Wang, F. Caruso, *Adv. Mater.* **2001**, *13*, 350.
[47] J. P. Ge, Y. D. Yin, *Angew. Chem. Int. Ed.* **2011**, *50*, 1492.